# Rutherford cable made of internal magnesium diffusion MgB$_2$ wires sheathed with Al-Al$_2$O$_3$ particulate metal matrix composite

P Kováč[1] , L Kopera[1], J Kováč[1], M Hain[2], T Melišek[1], M Kulich[1] and
I Hušek[1]

[1] Institute of Electrical Engineering, Slovak Academy of Sciences, Dúbravská cesta 9, 841 04 Bratislava,
Slovakia
[2] Institute of Measurement Science, Slovak Academy of Sciences, Dúbravská cesta 9, 841 04 Bratislava,
Slovakia

E-mail: Pavol.Kovac@savba.sk

## Abstract

Rutherford MgB$_2$ cable has been made from 12 single-core wires prepared via the internal
magnesium diffusion process with a light outer sheath of Al-Al$_2$O$_3$ particulate metal matrix
composite. Initially, critical currents of single-core wires with different diameters (between 1 mm
and 0.465 mm) were measured. X-ray tomography was applied for the analysis of the uniformity
of a Rutherford cable assembled of 0.465 mm strands. The obtained engineering current density
at 4.2 K and 6. 5 T for the present cable (with only 9.6% of MgB$_2$) is ∼3.6 times higher in
comparison with a similar cable fabricated via the powder-in-tube *in situ* process with 19.8% of
MgB$_2$ phase. The strain tolerance of the cable by bending has shown a critical diameter of
70 mm. AC losses measured via the calibration-free method have shown apparently lower
coupling losses for the cabled conductor. The obtained results are promising for future
lightweight, mechanically flexible and low AC loss MgB$_2$ superconductors suitable especially
for motors or generators.

Keywords: MgB$_2$, IMD process, Rutherford cable, Al stabilization, critical currents, bending
strains, AC losses

(Some figures may appear in colour only in the online journal)

## 1. Introduction

Some superconducting devices require high currents and also
flexible behaviour, which leads to the demand for cable
assembly. In all existing large particle accelerators (Tevatron,
HERA, RHIC, LHC) the main superconducting magnets are
based on Rutherford cables [1]. The Rutherford cable has
played a key role in accelerator magnet technology thanks to
its excellent mechanical, electrical and thermal properties.
These cables are also ideal for other magnets because they are
characterized by having strands that are fully transposed with
respect to the magnetic field, a significant compaction that

assures a large engineering critical current density and a
geometry that allows efficient winding of the coils [1]. A
typical cross-section of a Rutherford cable with rectangular
geometry provides both the highest strand packing density
and a flexible cable for the winding of coils with various
geometries and racetracks coils [2]. The work on Rutherford
cables based on some other superconductors, such as
BSCCO-2212, is also in progress [3, 4]. Up to now, MgB$_2$
cables were developed with different geometries: twisted and
braided cables [5–10], Roebel [9], and also Rutherford flat
cables [11, 12]. It was shown that non-reacted composite
wires can easily be cabled with standard cabling techniques

[6–9]. Cables giving an opportunity for complex structures using mono- or multi-core strands or a mixture of strands with stabilizing and/or reinforcing wires might have been the most attractive for winding applications. In addition, flat cables allow a decrease in bending diameters due to the small distance of strands from the cable neutral axis [11, 12]. Generally, AC losses of superconductors have three main contributions: (i) hysteresis losses, (ii) coupling losses, and (iii) eddy current losses in metallic components. Hysteresis losses can be suppressed by applying thin filaments, coupling ones by inter-filament or inter-strand resistivity and eddy currents by using a resistive sheath. It was found that for a cable made of mono-core wires, the hysteretic loss is dominant [13]. To reduce coupling losses, a transposition of the strands or filaments is needed. Taking into account undesirable degradation of transport currents due to the twisting process, the cable allows the lowest AC losses due only to hysteretic character and no deterioration of transport properties by cabling [13, 14]. In the cables, the transposition length and resistance between strands can be modified and consequently coupling currents and AC losses considerably reduced, which was already demonstrated by the comparison of AC losses of wire with twisted filaments with transposed strands in a circular cable [13]. Since the tolerable bending strain is a function of wire diameter, thin wires are more suitable for cables, also favoring short transposition lengths. Depending on the individual wire architecture, a strong degradation of the transport currents may be observed when reducing the size to very small filament diameters. This problem can be solved by using cables made of thin wires with fewer filaments [15]. For cabling purposes, $MgB_2$ wires made via the powder-in-tube *in situ* process are the best candidates to realize a drawing up of small diameters and transposition of strands before reaction treatment without damage [7, 11, 12]. In contrast to *in situ* wires, the wires made by internal diffusion of magnesium into boron (IMD) offer considerably higher current density [16], but are more sensitive to the deformation process because the uniform ratio of Mg core to boron powder is decisive for the created $MgB_2$ layer and its final current-carrying properties [17]. Our recent paper [18] has presented the basic properties of $MgB_2$ wire with lightweight sheath material manufactured by the IMD process, where Al-reinforced by $Al_2O_3$ material was for the first time successfully utilized. Al with $Al_2O_3$ is used due to effective mechanical reinforcement allowing successful wire deformation, which is not possible with too soft pure Al [19]. Al-sheath used for $MgB_2$ wires is motivated by a considerably lower mass of Al ($2.6\,\mathrm{g\,cm^{-3}}$) in comparison to copper ($8.9\,\mathrm{g\,cm^{-3}}$), which allows the reduction of the coil's mass. Low mass is an important issue for powerful off-shore wind turbines [20], airborne engines [21] and any application in space [22].

The aim of the present work is to show the properties of the first Rutherford cable assembled from $MgB_2$ wires with very light Al-$Al_2O_3$ outer sheet made via the IMD process.
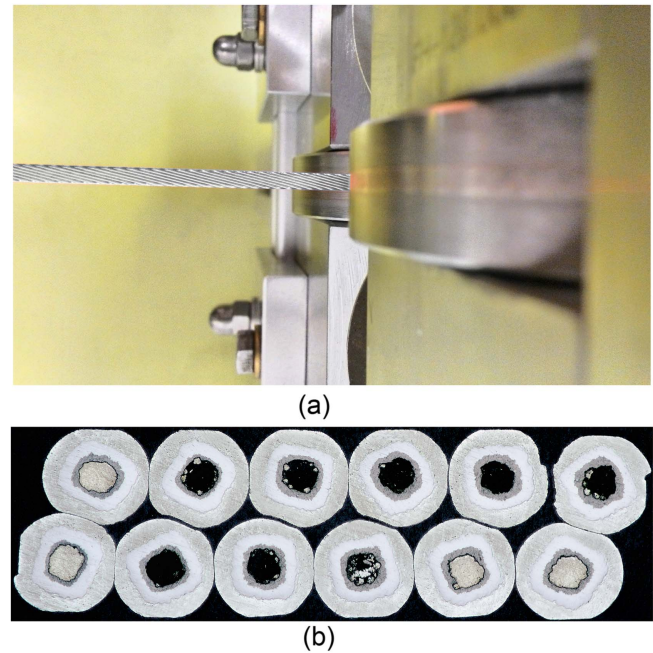


**Figure 1.** Rutherford cable of $0.85 \times 2.9$ mm outgoing from driven two-axial forming roller (a) and cross-section of heat treated cable at $630\,°C/10$ min observed by optical microscope (b).

## 2. Experimental

Single-core $MgB_2$ wire was composed of pure Mg wire of 2.94 mm in diameter surrounded by boron powder (purity 99.8%, $<1\,\mu m$, filled in glove-box) inside the Ta tube of diameters 5.6 mm 7.11 mm. The Mg/B/Ta composite was rotary swaged down to 6.0 mm and inserted into an Al + 1.37 vol.% $Al_2O_3$ metal matrix composite [18] tube of diameters 6.2 mm 9.1 mm, further swaged to 7.55 mm, then groove rolled to rectangular wire of 1.04 mm and finally cold drawn down to a diameter of 0.465 mm and a total length of 92 m. Heat treatment $300\,°C/30$ min was applied during groove rolling deformation (at diameters 4.3 mm and at 1.4 mm) and after each 50% area reduction by drawing. The as-drawn wire consisting of rounded 11% Mg, 12% B, 27% Ta barrier and 50% Al MMC outer sheath was divided into twelve pieces and stranded into the Rutherford cable. Figure 1(a) shows the Rutherford cable with the length of transposition $L_t = 20$ mm outgoing from the driven two-axial forming roller.

X-ray micro-tomography measurement device GE Nanotom 180, equipped with nano-focusing x-ray tube, accelerating voltage V = 170 kV, I = $100\,\mu A$, acquisition time 0.5 s, was used for the non-destructive analysis of the as-deformed Rutherford cable. The tested cable sample was stepwise turned around the rotation axis at a small selected angle of $12'$ and total of 1800 x-ray projections were measured. After obtaining all necessary projections, the volume image was reconstructed based on the inverse Radon transformation, and the resulting 3D image allows the observation of the whole composite uniformity. A 3D volume reconstruction from the projections was done using
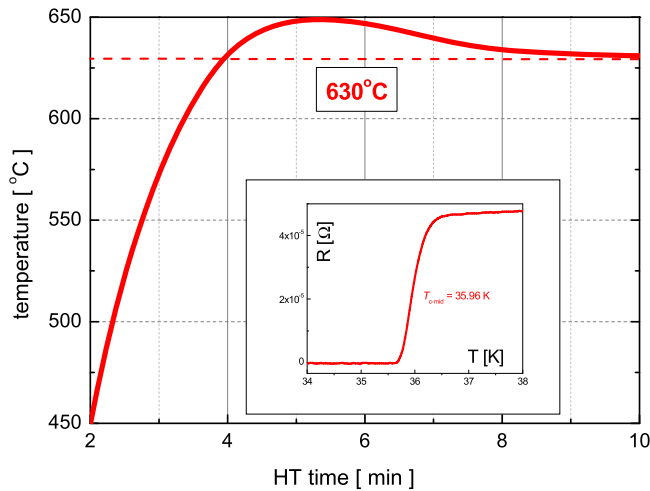
**Figure 2.** Temperature profile of applied heat treatment at 630 °C/ 10 min with the temperature holding time above 630 °C for 6 min. The insert shows the corresponding resistive transitions of MgB$_2$.

Datos|x-reconstruction software; rendering and segmentation of 3D image data were done in VGStudioMax 2.1.

The assembled Rutherford cable (12 × 0.465 mm) was finally annealed under argon atmosphere at 630 °C for 10 min by fast ramping; see figure 2. Optical microscopy was used for the characterization of composite elements after heat treatment. The volume composition in the heat treated wire of 0.465 mm corresponds to 11.4% of the central hole + residual Mg, 9.6% of MgB$_2$, 29.0% Ta and 50% Al MMC; see figure 1(b).

The resistive transition of the cable strand (0.465 mm) was measured by a standard four-probe method with DC current magnitude of 100 mA. Critical currents of cable strands at variable temperatures were measured in the PPMS system by AC transport option at the temperatures of 4.2 K, 10 K, 15 K and 20 K and also by DC transport measurement at 4.2 K. Transport critical currents of the whole cable were measured at liquid He temperature and external magnetic field between 4.0 T and 8.0 T using standard DC measurement with 1 $\mu$Vcm$^{-1}$ criterion. In the case of soldering, only the current contacts of the short cable sample, raised voltages (not originated from the superconducting transition) were measured due to non-identical strands resistance (corresponding current transfer). To perform the correct critical current measurements, strands in cable samples (∼70 mm long) were soldered together by WELCO 1134 solder containing 88% Cd and 12% Zn. This enabled measurement without any resistive voltages affected by current redistribution and to estimate $I_c$ correctly.

AC losses were measured via the so called 'calibration-free' method, which allows the experimental study of magnetization losses at temperatures between 18 and 40 K. A two-stage Sumitomo cryocooler and a heater with computer controlled power supply were used to keep the sample at constant temperatures during loss measurement. The sample holder consists of a high thermal conductivity aluminium nitride connected with the second stage of cryocooler by a flexible copper strand [13]. CdZn soldered and non-soldered

cable samples were measured and compared to see the effect of inter-strand coupling.

## 3. Results and discussion

Figure 1(b) shows the Rutherford cable with non fully identical 12 strands (especially the central parts), which is caused by Mg being not totally consumed in some of strands due to the small longitudinal variation of Mg/B ratio in as-drawn wire of total length 92 m (divided into 12 strands). Consequently, the heat treated and polished cables have some strands with central holes filled by Mg-spongy + polishing particles and it looks as though non-reacted Mg and other ones have black holes presenting empty spaces with fully consumed Mg for the created MgB$_2$ layer.

Figure 2 shows the real temperature profile applied for the heat treatment of cable samples and cable strands at 630 °C/10 min with Mg-Al eutectic temperature reached after 2 min. In reality, the duration at temperature 630 °C is only 6 min and the maximum temperature 648.8 °C still below the melting point of Mg (650 °C) and Al-Al$_2$O$_3$ metal matrix composite (652 °C). The insert in figure 2 shows the resistive transition of created MgB$_2$ phase with $T_{\text{c-mid}} \sim$ 36 K.

Figure 3 shows the pictures from x-ray micro-tomography focused on the Ta barriers of the as-deformed Rutherford cable. As can be seen from figure 3(b), the shape of the Ta barrier is nearly rectangular due to the applied groove rolling deformation from 7.55 mm to 1.04 mm; see also the cross-section in figure 1(b). The different hardness of individual composite elements during the deformation should be pointed out. While nearly constant HV0.05 micro-Vickers hardness ∼50 and ∼80 was measured for Mg-core and Al MMC sheath, respectively, apparent work hardening arising from 160 to 320 was observed for Tantalum. Moreover, the micro-hardness measurements of the Ta barrier in the final cable strands exhibited structural inhomogeneity. Further investigation showed that the tube used for the Ta barrier was not seamless but seam welded. Deformities in barriers showed in figure 3(b) are places in the seam welds where the microstructure of Ta is changed and exhibits different behavior than the unwelded region of the tube. Figures 3(c), (d) show the place of the interrupted Ta barrier at the cable edge where the weakened wall is exposed to higher and more complex stress. Consequently, during the final HT at 630 °C– 650 °C, the interrupted barrier can lead to local defects resulting from a reaction of the Mg core with the surrounding Al MMC sheath; see figure 4.

Figure 4 shows the local defect of one strand at the cable edge, where the interaction of Mg with Al has occurred through the interrupted Ta barrier during the heat treatment process. The Al-Mg binary diagram shows the maximum solubility of Mg in Al at eutectic temperature 450 °C [23]. In addition, Al$_3$Mg$_2$ compound is created from low temperatures (<100 °C) and therefore any direct contact of Al with Mg has to be avoided.

Figure 5 shows the critical currents (a) and critical current densities (b) of the cable strand measured by AC
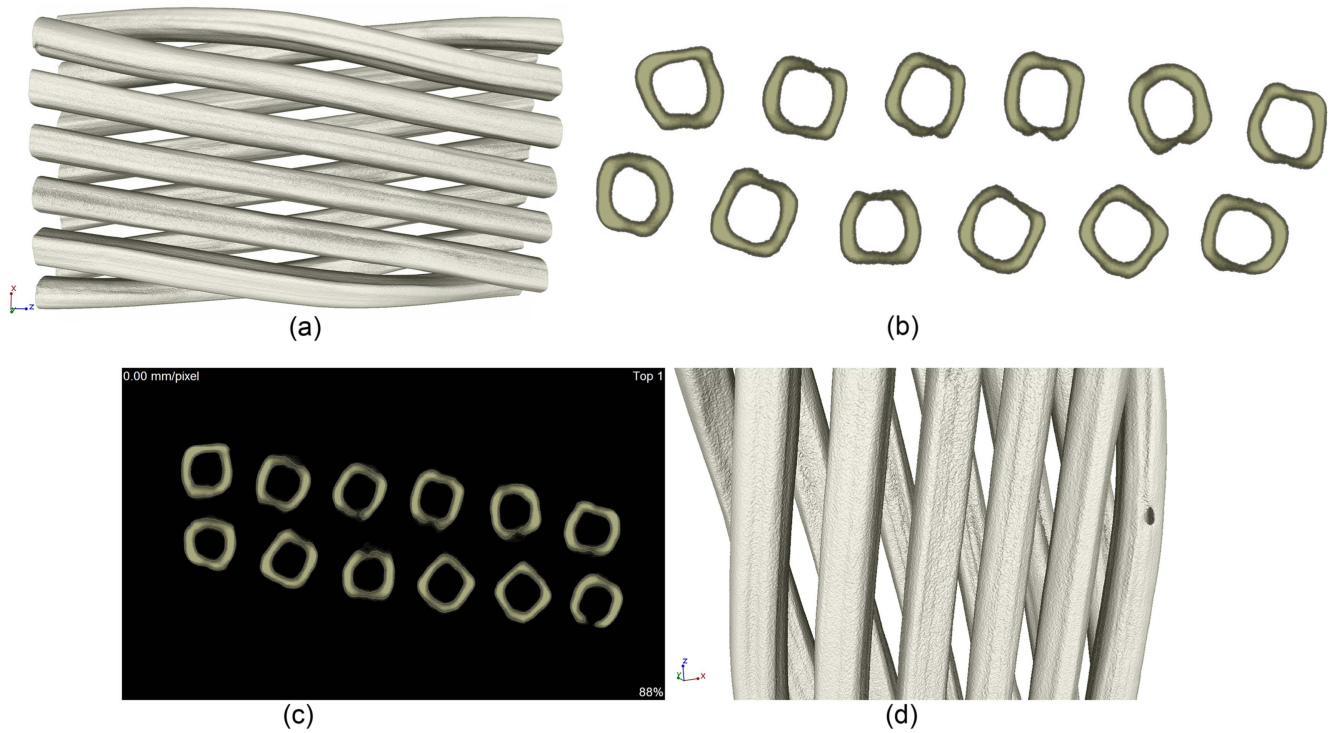
**Figure 3.** Ta barriers of as-deformed Rutherford cable observed by x-ray micro-tomography (a), transversal view showing the softened places in barrier tubes (b), broken barrier observed in the cable cross-section (c) related to 3D view (d).
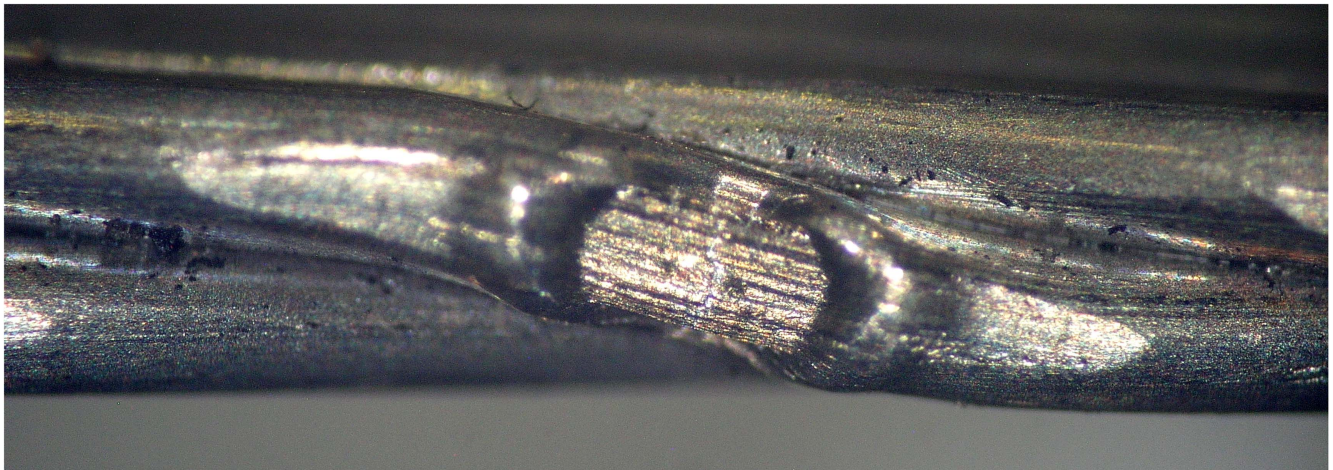


**Figure 4.** View of strand where a strong interaction between Mg and Al occurred during heat treatment.

transport option at temperatures between 4.2 K and 25 K. The AC option is limited by the maximum transport current 2 A, but it nonetheless allows one to estimate the current densities at the temperature range and compare them with $J_c$ of this wire composition of size 1.04 mm measured by VSM [18]. Figure 5(c) shows a very good $B_{10000}(T)$ correlation in the range of 4.2 K to 20 K for both wires (1.04 mm [18] and 0.465 mm). This means that the quality of MgB$_2$ layer was not affected by reduction of the wire diameter.

Figure 6(a) shows the critical currents of individual strand obtained by DC and AC transport measurements compared with $I_c$ of Rutherford cable 0.85 × 2.9 mm. One can see good agreement between DC and AC transport data and also identical $I_c$ of the Rutherford cable with the current

of twelve strands at external field of 8 T. This means that the cabling process does not deteriorate the density of the boron layer. Slightly decreased critical currents of Rutherford cable in comparison to the hypothetical one (12 × $I_c$ of strand) in low fields can be caused by an increased self-field effect and by more apparent current redistribution among the strands. Figure 6(b) compares the engineering current density of the non-doped *in situ* Rutherford cable [12] with the present IMD one. While $J_e = 10^4$ Acm$^{-2}$ was measured at 3.25 T for the *in situ* cable with 19.8% of MgB$_2$ phase, the same $J_e$ was measured at 4.75 T for the IMD cable with only 9.6% of MgB$_2$. It demonstrates the promising capability of the IMD cable for very high engineering current densities. Cable thickness reduction from 0.85 to 0.8 mm (by 5.8%) increased
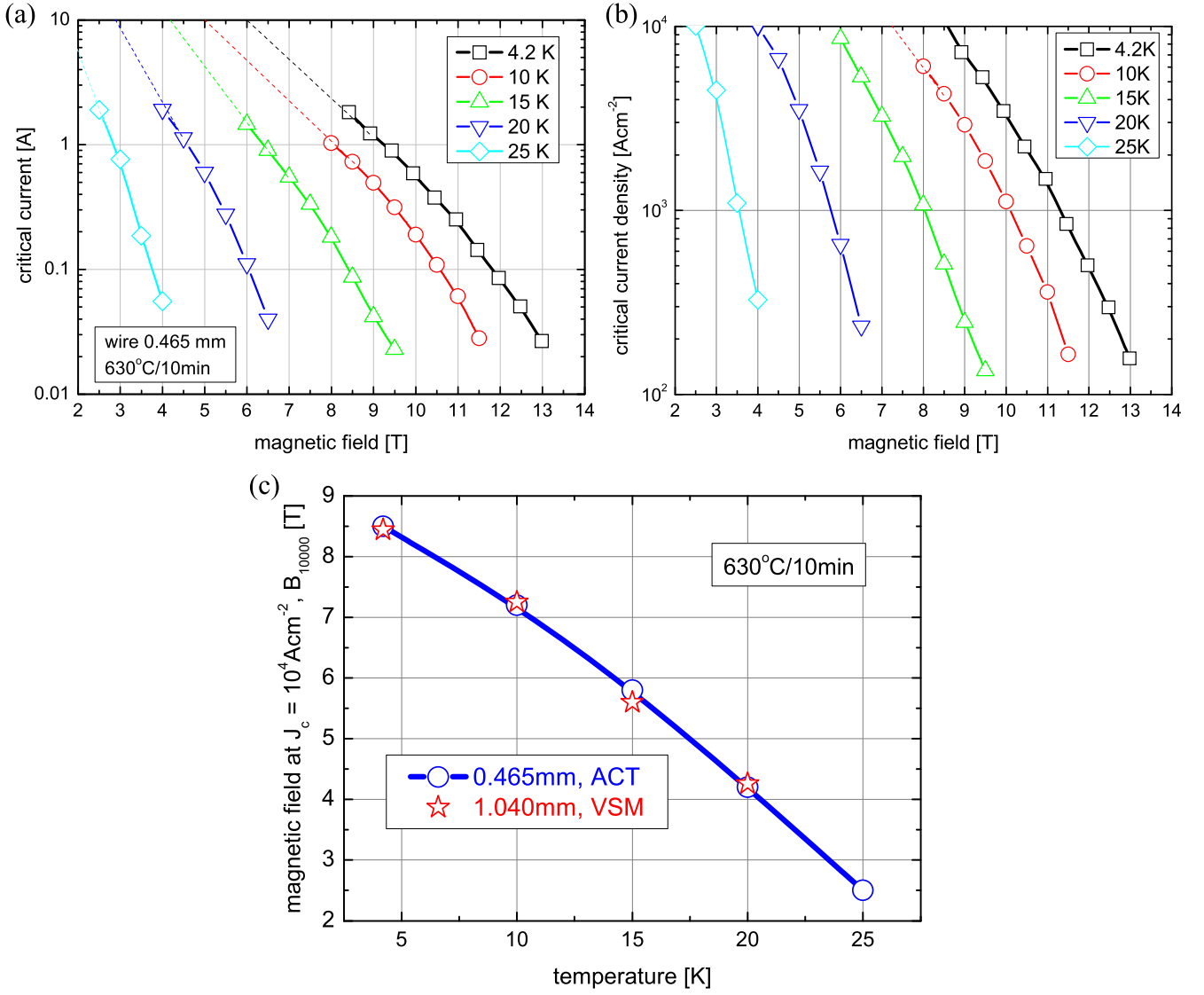
**Figure 5.** Critical currents (a) and current densities (b) of the 0.465 mm wire used for cabling. The values of external magnetic field $B_{10000}$ versus temperature at which $J_c = 10^4$ Acm$^{-2}$ is reached (c).
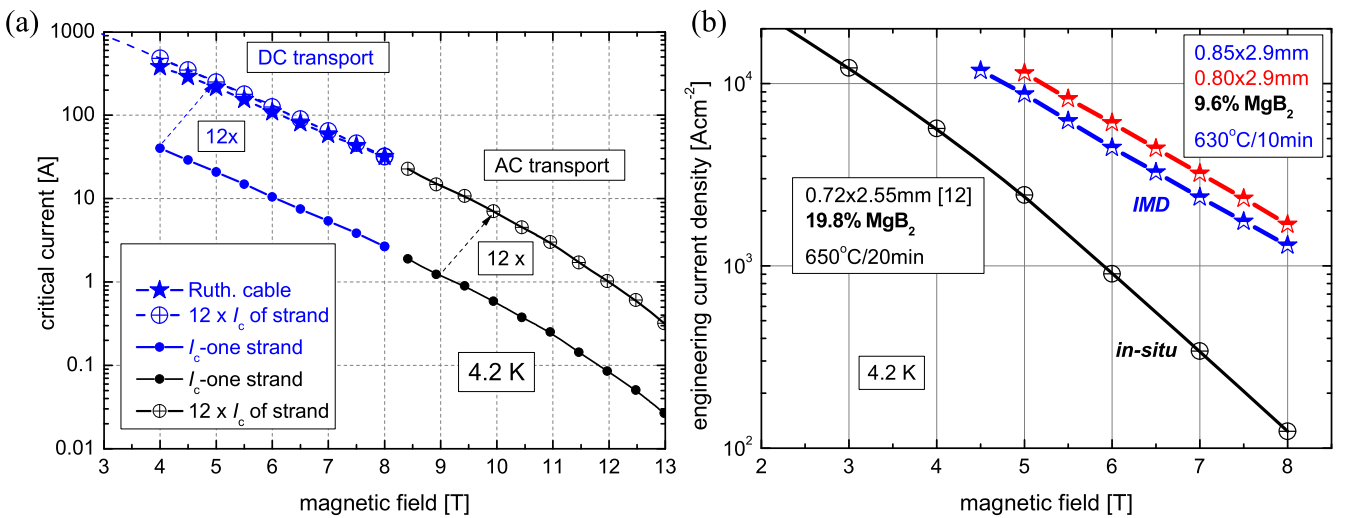


**Figure 6.** Critical currents of Rutherford cable (stars) compared with currents of strand (circles) measured by DC (blue) and AC transport (black) measurements (a) and comparison of engineering current density of the present IMD cable with Rutherford cable made of 12 *in situ* strands 0.39 mm in diameter (b).
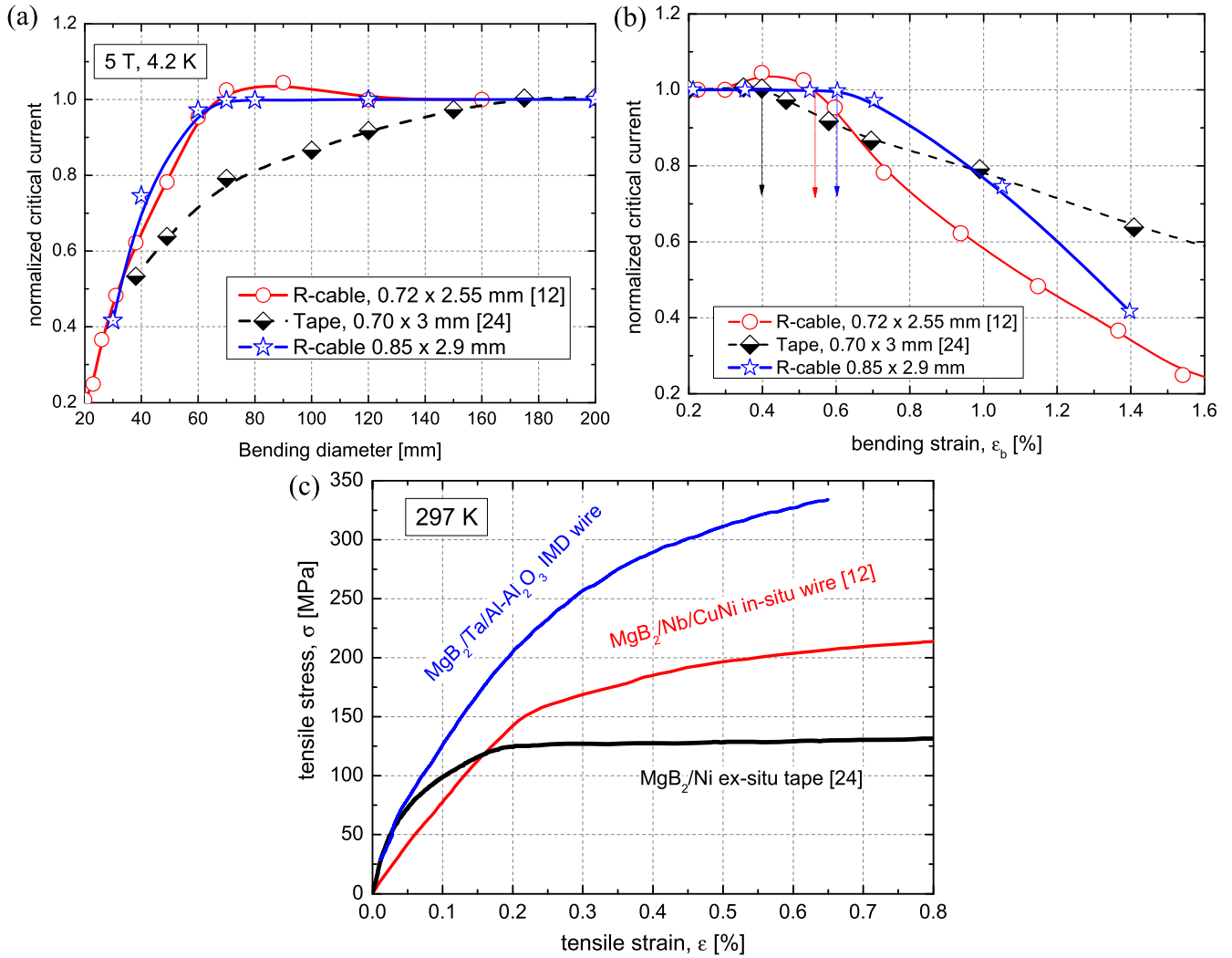
**Figure 7.** Normalized critical currents of two Rutherford cables bent to variable diameters compared with $I_c$ degradation of 0.7 mm thick MgB$_2$ tape (a), corresponding $I_c$ degradation versus the bending strain (b) and the stress-strain characteristics of cable's strands and Ni sheathed tape (c).

$J_e$ by 36. 7%, which is in agreement with the effect of boron densification observed for the cable made of *in situ* wires, where $J_e$ was doubled after applying ~10% thickness reduction [12]. A higher degree of densification has not been applied due to weakened Ta barriers (see figure 3) and their possible breaking.

Figure 7(a) shows a comparable tolerance to bending strains for Rutherford cable 0.72 × 2.55 mm made of *in situ* strands of diameter 0.39 mm [12] with the present 0.85 × 2.9 mm one. Both cables show the beginning of critical current degradation below the bending diameter 70 mm, less than 5% degradation at 60 mm and similar $I_c(d_b)$ dependences bellow 70 mm. Although the Cu10Ni sheathed *in situ* cable shows a certain current improvement at bending diameters around 90 mm, this effect is not present for the IMD cable, which may be attributed to different residual strain inside the Al-Al$_2$O$_3$ sheath. The $I_c(d_b)$ characteristic observed for monolithic *ex situ* MgB$_2$ tape of even lower thickness with Ni sheath shows the critical current degradation that starts at a much higher bending diameter ~170 mm

[24]. Due the differing sizes of the compared cables' strands and tape thickness, the degradation of critical current versus bending strain has been evaluated.

The following equation has been used to estimate the bending strain in compared samples: $\varepsilon_b = h_s/(d_b + h_s)$, where $h_s$ is the strand size or tape thickness and $d_b$ the applied bending diameter.

Figure 7(b) shows how the critical current is degrading with the bending strain. While the beginning of the critical current degradation was measured at $\varepsilon_b = 0.4\%$ for *ex situ* made MgB$_2$ tape, $\varepsilon_b = 0.54\%$ and 0.6% are estimated for *in situ* and IMD Rutherford cable, respectively. It has already been reported that the strength of the outer sheath material has a dominant effect on the bending strain tolerance of MgB$_2$ wires [25]. Figure 7(c) shows the stress-strain characteristics of the cable's strands and Ni sheathed *ex situ* tape measured at room temperature. One can see that tolerances to bending strain in figures 7(a) and (b) correspond to the mechanical properties of these wires. It can be concluded that the best connected MgB$_2$ grains prepared by the IMD process,
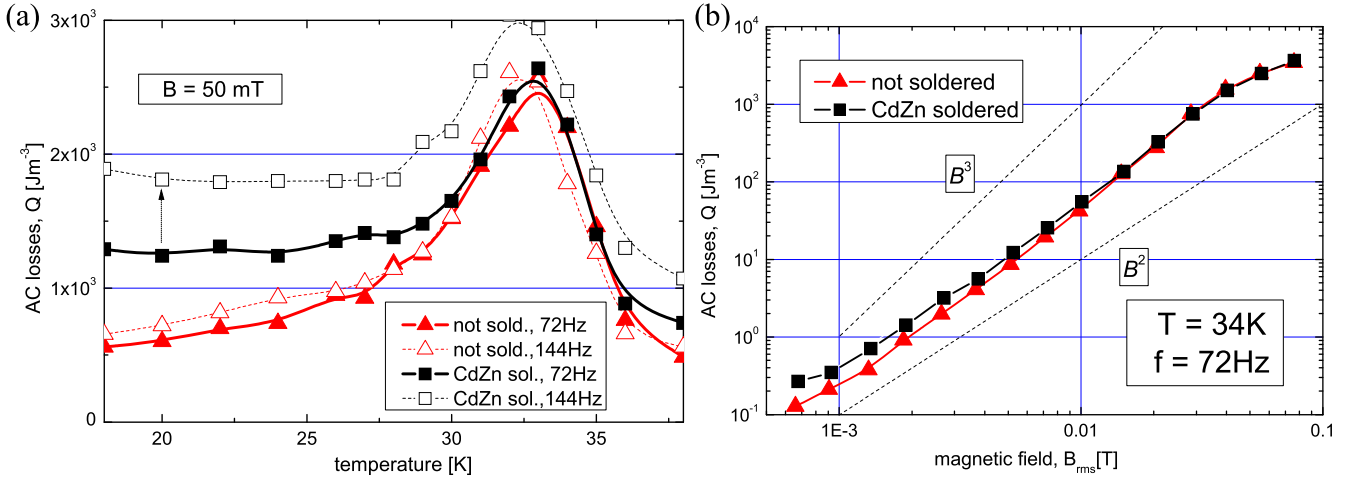
**Figure 8.** The temperature dependences of AC losses for CdZn soldered and not soldered Rutherford cable 0.85 mm × 2.9 mm measured at two frequencies 72 and 144 Hz (a) and field dependence of Q at temperature 34 K and frequency 72 Hz (b).

combined with a low heat treatment temperature (~640 °C) at which hardness of the outer Al-Al$_2$O$_3$ MMC sheath still remains high, are responsible for a good strain tolerance of the present Rutherford cable.

Figure 8(a) shows AC losses normalized per whole volume of the Rutherford cable 0.85 mm × 2.9 mm at the temperature range of 18–38 K. The AC loss maximum close to 33 K corresponds to full field penetration of MgB$_2$ core made by IMD process [26]. Relatively large AC losses are measured below 30 K and also above the critical temperature (>36 K), which indicates some contribution of eddy current loss in the outer Al-Al$_2$O$_3$ sheath. While the AC losses of the non-soldered cable decrease with lowered temperature and the effect of higher frequency is negligible, considerably increased losses can be seen for the soldered one due to increased coupling losses. The effect of additional eddy current losses inside the CdZn solder can be observed from the measurement at different frequencies, especially at temperatures above the critical one ($T_c \sim 36$ K). AC loss of soldered cable at 144 Hz is increased in the whole temperature range (see figure 8(a)), which is a result of higher coupling and eddy current loss. At the low temperatures of 18–25 K, the effect of the higher frequency is more significant as a result of dominating coupling current losses, which are not visible above $T_c$. The resistivity of the Al-Al$_2$O$_3$ sheath and CdZn solder has been measured at 25 K and values of $1.5 \cdot 10^{-9}$ Ωm and $3 \cdot 10^{-9}$ Ωm were obtained for using Al-Al$_2$O$_3$ and CdZn, respectively. Eddy current losses are inversely proportional to the resistivity of metallic layers and proportional to the second power of the frequency:

$$Q_{\mathrm{eddy}} \sim tw f^2 / r$$

where $\rho$ is the resistivity of metallic material, $f$ is frequency and $t$ and $w$ and are thickness and width [27]. Coupling losses at low frequencies are proportional to the time constant:

$$\tau = \mu_0/2\rho_{\mathrm{ef}}(L_{\mathrm{p}}/2\mathrm{p})^2$$

where $L_{\mathrm{p}}$ is the length of transposition and $\rho_{\mathrm{ef}}$ is effective inter-filament (strand) resistivity [28]. The effective inter-

strand resistivity of aluminum sheathed (and naturally oxidized) Rutherford cable is much larger than for soldered strands. Lower coupling and eddy current losses in the non-soldered cable demonstrate clearly the possibility of decreased total losses of Rutherford cables in comparison to a monolithic multi-core wire of similar diameter.

Figure 8(b) confirms the considerable contribution of coupling and eddy current losses into the total loss of MgB$_2$/Ta/Al–Al$_2$O$_3$ cable via the quadratic increase of AC losses with field (~$B^2$). Typically only hysteresis AC losses have behaviour proportional to ~$B^3$. The possible reduction of eddy current losses in the present cable can be obtained via the utilization of an outer sheath with higher content of Al$_2$O$_3$, which increases the resistivity of Al–Al$_2$O$_3$ material and reduces corresponding eddy current losses [29].

## 4. Conclusions

The first Rutherford cable has been made from 12 single-core MgB$_2$ wires made via the IMD process with very light Al-Al$_2$O$_3$ MMC outer stabilization sheath. The engineering current density of Al sheathed cable with 9.6% of MgB$_2$ phase fabricated by IMD process is 3.6 times higher (at 4.2 K and 5 T) in comparison with an *in situ* made Rutherford cable with 19.8% of MgB$_2$. The presented cable allows bending to the diameter of 70 mm without any critical current degradation. Lowered AC loss of the Rutherford cable in comparison to a monolithic wire is demonstrated due to supressed coupling current losses. In the case of the usual volume of outer sheath at 50% and the same cable size, barrier material and MgB$_2$ content, the estimated mass ratio between the Cu and Al sheathed cable will be 1.73. The presented Rutherford cable shows promising potential for future manufacturing of flexible and low AC loss MgB$_2$ superconductors suitable especially for light superconducting motors or generators, e.g. for powerful off-shore wind turbines, airborne engines and for space applications.

## Acknowledgments

## ORCID iDs

P Kováč ⬤ https://orcid.org/0000-0003-1872-0359

## References

[1] Cabanes J *et al* 2016 *Cryogenics* **80** 333
[2] Dietderich D R and Godeke A 2008 *Cryogenics* **48** 331
[3] Collings E W *et al* 1999 *Supercond. Sci. Technol.* **12** 87
[4] Andreev N *et al* 2007 *IEEE Trans. Appl. Supercond.* **17** 1027
[5] Musenich R, Greco M, Razeti M and Tavilla G 2007 *Supercond. Sci. Technol.* **20** 235–8
[6] Kováč P, Hušek I and Melišek T 2008 *Supercond. Sci. Technol.* **21** 125003
[7] Holúbek T, Schlachter S I and Goldacker W 2009 *Supercond. Sci. Technol.* **22** 055011
[8] Kováč P, Hušek I, Rosová A, Melišek T and Kopera L 2010 *Supercond. Sci. Technol.* **23** 105006
[9] Hušek I, Kováč P, Melišek T and Kopera L 2009 *Cryogenics* **49** 366–70
[10] Hossain M *et al* 2014 *Supercond. Sci. Technol.* **27** 095016
[11] Kopera L, Kováč P, Hušek I and Melišek T 2013 *Supercond. Sci. Technol.* **26** 125007
[12] Kopera L, Kováč P, Kulich M, Melišek T, Rindfleisch M and Hušek I 2017 *Supercond. Sci. Technol.* **30** 015002
[13] Kováč J, Šouc J, Kováč P, Hušek I and Gömöry F 2013 *Physica* C **495** 182
[14] Kováč P, Hušek I, Kováč J, Melišek T, Kulich M and Kopera L 2016 *IEEE Trans. Appl. Supercond.* **26** 6200705
[15] Schlachter S 2016 *MgB₂ Superconducting Wires* ed R Flukiger (New Jersey: World Scientific) p 549
[16] Li G Z, Yang Y, Susner M A, Sumption M D and Collings E W 2012 *Supercond. Sci. Technol.* **25** 025001
[17] Higashikawa K, Yamamoto A, Kiss T, Ye S, Matsumoto A and Kumakura H 2014 *Physica* C **504** 62
[18] Kováč P, Hušek I, Melišek T, Kulich M, Rosová A, Kováč J, Kopera L, Balog M, Krížik P and Orovčík Ľ 2017 *Supercond. Sci. Technol.* **30** 115001
[19] Balog M, Simancik F, Walcher M, Rajner W and Poletti C 2011 *Mater. Sci. Eng.* A **529** 131–7
[20] Marino I, Pujana A, Sarmiento G, Sanz S, Merino J M, Tropeano M, Sun J and Canosa T 2016 *Supercond. Sci. Technol.* **29** 024005
[21] Masson P J, Nam T, Choi T and Luongo C A 2009 *IEEE Trans. Appl. Supercond.* **19** 1662
[22] Spillantini P 2010 *Adv. Space Res.* **45** 900
[23] Massalski T B, Okamoto H, Subramanian P R and Kacprzak L (ed) 2001 *Binary Alloy Phase Diagrams* fourth printing (Materials Park, OH: ASM International)
[24] Kováč P, Kopera L, Melišek T, Sarmiento G, Sanz S, Brisigotti S, Nardelli D and Tropeano M 2015 *IEEE Trans. Appl. Supercond.* **25** 6200607
[25] Kováč P, Hušek I, Melišek T, Kulich M and Kopera L 2016 *Supercond. Sci. Technol.* **29** 045002
[26] Kováč J, Šouc J, Kováč P and Hušek I 2015 *Supercond. Sci. Technol.* **28** 015013
[27] Grilli F, Pardo E, Stenvall A, Nguyen D N, Yuan W and Gömöry F 2014 *IEEE Trans. Appl. Supercond.* **24** 8200433
[28] Kwasnitza K and Clerc S 1994 *Physica* C **233** 423
[29] Kováč P, Balog M, Hušek I, Kopera L, Križik P, Rosová A, Kováč J, Kulich M and Čaplovičová M 2017 *Cryogenics* **87** 58